NOISE ESTIMATION IN PANORAMIC X-RAY IMAGES: AN APPLICATION ANALYSIS APPROACH*

Peter M. Goebel[1,2]*, Student Member IEEE, Ahmed N. Belbachir*[1]*, Member IEEE, Michael Truppe*[3]

[1]Vienna University of Technology, Pattern Recognition and Image Processing Group, Vienna, Austria
<nabil,goe>@prip.tuwien.ac.at, http://www.prip.tuwien.ac.at
[2]fh-campus wien, Technical Process and Project Management, Vienna, Austria
[3]Karl Landsteiner Institute for Biotelematics, Danube University Krems, Austria
mtruppe@biotelematics.at, http://www.biotelematics.at

ABSTRACT

This paper presents an appropriate approach for the robust estimation of the noise statistics in dental panoramic X-ray images. To achieve maximum image quality after denoising, a semi-empirical scatter model is presented, leading to a local adaptive Gaussian Scale Mixture (GSM) model. State of the art methods use multiscale filtering of images to reduce the irrelevant part of information, based on generic estimation of noise. The usual assumption of a distribution of Gaussian and Poisson statistics only leads to overestimation of the noise variance in regions of low intensity (small photon counts), but to underestimation in regions of high intensity and therefore to non-optimal results.

The analysis approach is tested on a database of 50 panoramic X-ray images and the results are cross-validated by medical experts. It is shown that the local standard deviation (SDEV) in images, stemming from homogeneous phantoms (Al, PMMA), follows a Generalized Nakagami Distribution (GND). The heavily tailed distribution is not covered entirely by the GND. The error density function, is hypothesized to stem from scatter-glare, degrading the image. A beam stop method, for estimation of the scatter-glare amount, verifies that hypothesis. Finally, the application of the method for a phantom image, is shown with denoising results for comparison purpose, followed by the conclusion.

Keywords: Noise Estimation, De-noising, Nakagami-m

1. INTRODUCTION

In medical diagnostics intuitive decisions take place, based on experience, beside medical knowledge. Appropriate methods have to deal with the detection of small, low contrast image details, situated side by side, probably not differing in gray-level-mean, but may having slightly different variance. Denoising with overestimated noise variance easily removes such details, whereas doing it with underestimated once, keeps the noise. Some attempts of authors to preserve the edges within an image fail in the case of low contrasts.

Among others, the most used method for image denoising is multiscale filtering based on the wavelet transform [15, 17]. The basic idea is to decompose an image into an over complete representation with different contributions in several frequency bands and at different scales. Thus, the deterministic image content is represented by a set of few strong coefficients, whereas the noise is spread over all coefficients with weakly strength. A deconvolution technique is usually applied using linear or non-linear filtering [4, 15] to reduce the contribution of noise in the transformed coefficients. In [14] a combined method for denoising and deblurring is given, using Gaussian Scale Mixtures (GSM). The works in [2] evaluate the efficiency of denoising and enhancement of X-ray images by simulating additive noise of known distribution. However, X-ray images show neither Gaussian nor Poisson distributions alone, because such noise is coherent to the density of matter, leading to spatially varying variance of the noise.

Dental Panoramic Radiography (DPR) is a technique where the entire dentition is projected onto a sensing device. The physics of such a radiographic process can be subdivided into X-ray source, interaction of the beam with matter and imaging of the remaining photons. Source and detector are in opposition, rotated around the patients head. The focal area of the X-ray beam describes a planar curve, which is standardized for the human teeth and jaws. From the primary polyenergetic X-ray beam, photons are absorbed (i.e. scattered) along the path between the source and detector by the patient's matter (muscle, fat, bone, air, or contrast agents). The photon attenuation of each type of matter depends on its elementary and chemical composition as well

*THE APPROACH WAS SUPPORTED BY DUERR DENTAL, GERMANY, IN MANUFACTURING THE DEDICATED AL AND PMMA PHANTOMS, AND IN THE ACQUISITION OF THE TEST IMAGES, WHERE THE SUPPORT FROM MR. H. HAENTSCH IS EXPLICITLY ACKNOWLEDGED.

as the beam. This effect is quantified by the mass attenuation coefficient (MAC). The MAC gives the fraction of photons that are absorbed by unit thickness of matter and varies with photon energy, too. The interesting energy range for diagnostic DPR is about $8keV$ to $90keV$, where three main scatter processes are relevant: a) Photoelectric absorption, b) coherent scatter and c) incoherent (i.e. Compton) scatter [1, 8, 5]. Image degradation is caused by deflected primary photons due to scattering events, which still reach the sensor, resulting in scatter-glare. A deeper introductory chapter is given in the companion paper from the authors [5].

The estimation of noise itself is left open by many authors. A comparative study between six methods is shown in [10]. A method for blind estimation of noise variance is given in [9] and the references herein. Statistical models for images are described in [13], in [14] the application of Gaussian Scale Mixtures to natural images is given.

What can be concluded from the above is that an accurate investigation on the noise model has to be performed for optimal denoising results. The implemented semi-empirical probabilistic scatter model is verified by data from NIST database [8] and applied to a comparison with real image acquisitions from appropriate homogeneous phantoms (i.e. Poly(Methyl Methacrylate) (PMMA) and an Aluminum step-wedge).

The structure of the paper is as follows: in Chapter 2, the problem statement is given, followed by a description of the proposed approach in Chapter 3. In Chapter 4 the analysis and results are shown, Chapter 5 states the conclusions of the work.

2. PROBLEM STATEMENT

The goal is to find better estimates for the noise variance in panoramic X-ray images. To illustrate the problem, a degradation of the image quality by adding a mixture of Gaussian and Poisson noise to a CT image is shown in Fig. 1 (left). A classical denoising approach is performed by wavelet coefficients soft-thresholding using an usual noise estimate [4](right). The noise is mainly removed, but the image is blurred. Within the weak wavelet coefficients there is hidden edge information, therefore fine details in the image are lost (pseudo-Gibbs phenomenon).

Fig. 2 shows the effect of such a denoising on the real image. The low contrast image (left) is more sensitive to the overestimated noise estimate than the CT image .

3. THE PROPOSED APPROACH

In the proposed approach, prominent constraints are: a) preservation of the image's overall look; b) preservation of the diagnostic content in the image; and c) detection of small, low contrast details in the diagnostic content of the image.

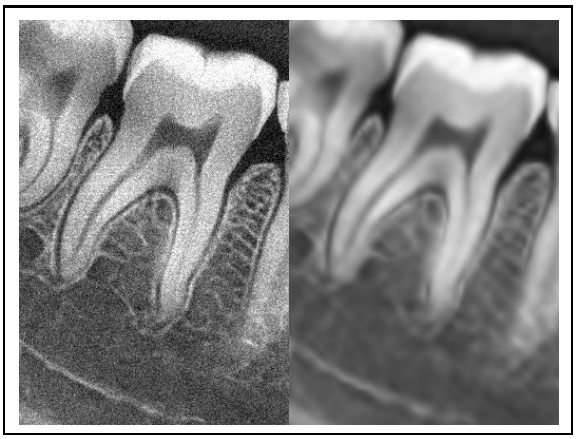

Fig. 1. The zoomed CT image: artificial Gaussian and Poisson Noise added (left); and classically denoised (right).

Fig. 2. A zoom of the real image (left) and it's classically denoised variant (right).

As shown in the previous section, state of the art methods provide non-convincing results. The new approach is founded on an attempt to interpret the problem from the view of blind source separation (BSS), thus to see the panoramic image as a sample mixture of (unwanted) background information, diagnostic information and noise. The question is, how to get another sample image? Due to the fixed setup condition of a dental panoramic acquisition system, an empty scan, taken without patient can provide another good sample - the image of the illuminating background. This background image gives information on the non-uniform X-ray illumination and also owns the particle statistics, given from the X-ray source, collimation and prefiltration of the beam. Several background estimates, to cover all relevant diagnostic operating modes, may be acquired offline and stored for instant use.

Following a classical approach for denoising [4], using

an overcomplete wavelet decomposition and thresholding of the wavelet coefficients by a threshold calculated from a noise estimate, leads to the application of denoising for dental panoramic X-ray images. With respect to the coherent noise problem explained, an artificial spatial noise map model is generated, which can be thought as a one-to-one realization of any type of noise (additive or multiplicative as well) within the original image. Thus, the proposed method for estimation of noise can be used to give better than usual noise estimates, which includes the effects of varying scatter-glare noise, too. In the following subsection, the estimation model is described, followed by the description of a physical setup to bring up the ground-proof for the model, estimated. Selected results from the experiments are shown in the next chapter.

3.1. The Noise Estimation Model

A semi-empirical model for the generation of a spatially adaptive noise map is implemented under some simplifying conditions, which is cross checked with data from the NIST database [8] and Monte Carlo simulations by the GEANT4 simulation package.

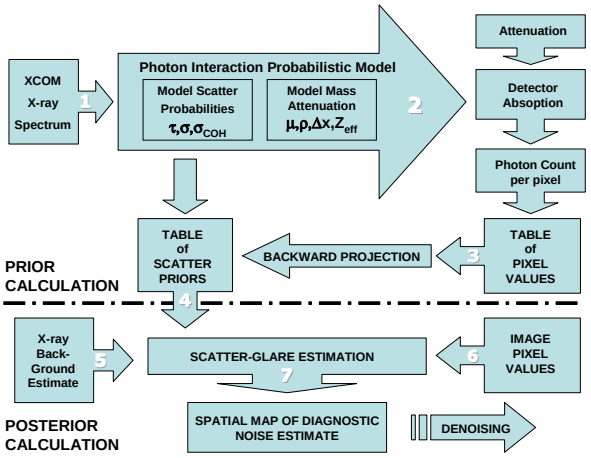

Fig. 3. The Estimation Model has two majors: the upper one is for the calculation of the scatter prior table, whereas the lower one is for the posterior processing of an actual image.

Fig. 3 shows an overview of the estimation model, which itself is a composition of several modeling parts. It is subdivided into a prior calculation part and a posterior one.

For the prior part, the *X-ray energy spectrum* E **-1-** is calculated by a semi-empirical model [3], which is the input to the *photon interaction probabilistic model* **-2-**. In that, three simplifying assumptions are made: a) Compton scatter σ_{incoh} is assumed to be constant; b) Coherent scatter σ_{coh}

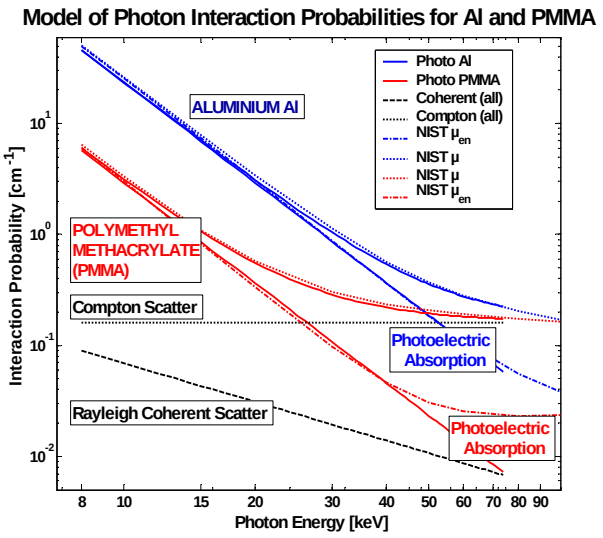

Fig. 4. The simplified Probabilistic Photon Scatter Model.

is modeled as Rayleigh scatter only and c) both assumed to be independent of the effective atomic number Z. Photoelectric scatter τ varies accordingly to the fraction of $\frac{Z^4}{E^3}$. After attenuation and detector absorption, a photon count per pixel produces a *table of pixel values* **-3-**, which is inversely backward scatter projected. Thus generates the *table of scatter priors* **-4-**, which is used by the posterior together with the *background estimate* **-5-** and the actual *image pixel values* **-6-** to estimate the *scatter-glare* **-7-**, generating the spatially adaptive noise variance map.

In Fig. 4 the total scattering in terms of the linear attenuation coefficients $\mu = \tau + \sigma_{incoh} + \sigma_{coh}$ for aluminum and PMMA is related to scattering data from the NIST database [8] (dotted lines). Up to $40keV$ the energy mass attenuation coefficients μ_{en} are also in good relation to the modeled Photoelectric absorption τ. Above that point, the model has an upcoming difference, especially at softer matters (i.e. PMMA), but their interaction probability is quite low, thus the error may be neglected. However, the model does not claim to replace any of the Monte Carlo methods in terms of accuracy, but it generates an appropriate enough scatter prior.

The model developed is verified for the physical setup (Fig. 6 Filters 1..3), where in Fig. 5 the modeled results are compared to semi-empirical data from the NIST database [8], and again one can see the good conformity.

3.2. Physical Setup

Fig. 6 defines the physical setup for the verification of the estimation model. At the left hand side, the X-ray generator

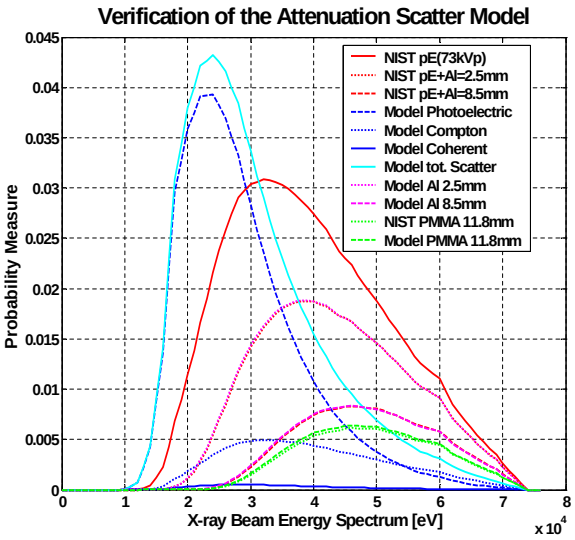

Fig. 5. The Attenuation Scatter Model in Verification.

is shown, which produces the X-ray beam, I_0. A prefiltering stage, Filtration 1 and Filtration 2, by 2.5 mm and 6 mm Aluminum, respectively, attenuates the beam to I_1. The diagnostic absorption by the patient's matter is simulated by Filtration 3 of PMMA. Finally, filtration by a 3mm lead, which has several holes of 3mm, is essential for the measure of scatter-glare and is only inserted temporally for measurement of that. The diagnostic image is gathered by an absorbing photo stimulable phosphor (PSP) plate ($BaFBrI : Eu^2$), which traps and stores the remaining photons.

Formulating the physical setup of Fig. 6 in mathematical terms of attenuation coefficients leads to:

$$I_2 = \underbrace{\underbrace{I_0 \cdot \exp(-\sum_{i=1}^{K=2}(\mu_{AL}\, d_i)}_{background\ scatter}}_{I_1} \cdot \underbrace{\exp(-\mu_P\, d_P)}_{diagnostic\ scatter} \qquad (1)$$

In (1) the intensity I_2 at the sensor is decomposed into the background part I_1, attenuated by the aluminum filters, attenuated further by the diagnostic part of interest, crossing the primary beam. Within the photon energy range, suitable for dental panoramic X-ray diagnostic, Photoelectric absorption, Coherent scatter and Compton scattering, induce the contrast function of matter [5], which forms the image.

$$\mu_p = -\frac{\ln\left(\frac{I_2}{I_1}\right)}{d_p} \qquad (2)$$

Calculating the logarithmic fraction, for the phantom inserted, from images I_2 and I_1 in (2), relating to its thickness

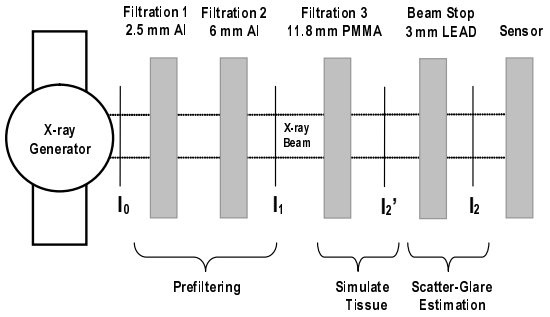

Fig. 6. Physical Setup for the Model

d_p, leads to the effective MAC μ_p, which is around 0.3 for the PMMA phantom plate.

4. THE ANALYSIS AND RESULTS

For the analysis, an aluminum step-wedge phantom and a PMMA flat phantom was constructed, which supports the ground-proof of the analysis.

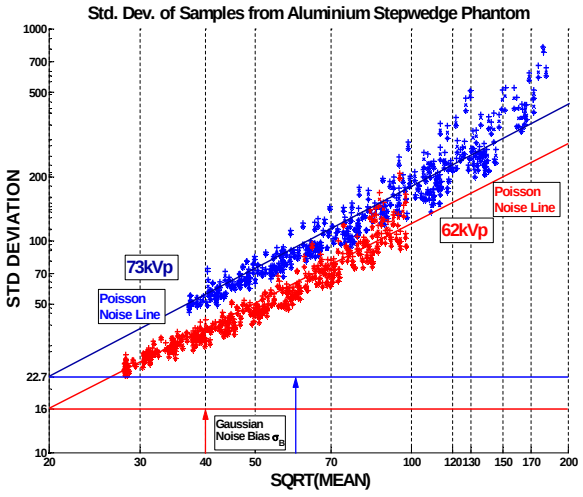

Fig. 7. A Scatter Plot of $SDEV$ for two operation modes.

Images from the step-wedge, inserted at the rightmost position in Fig. 6, are processed by (2) and the 9x9 local SDEV is plotted in Fig. 7 accordingly to the square root of the local mean. Two different operating cases are shown: one at 62 kVp and one at 73 kVp of the X-ray tube. For com-

parison, the Poisson equivalent gains $SDEV = \sqrt{MEAN}$ are drawn as lines for both cases, where one can see, the Gaussian bias σ_B for either mode and the increasing variance from the measured values toward higher mean values.

4.1. Fitting the Generalized Nakagami Density (GND)

Phenomena of discrete nature are described well by a Poisson distribution [11]. The waiting times between such Poisson events are Gamma distributed. From modeling of multipath fading channels in telecommunication and ultrasonic mammography characterisation of the backscattered echo, a scalable form of a Gamma type distribution, the Nakagami-m density function is known. The generalized Nakagami density function (GND) [12] is a type of Gamma density with three free parameters: Ω, m, and s, the scaling factor, the number of free degrees, and an additional shape adjustment parameter, respectively.

The Generalized Nakagami-m distribution is given by:

$$f\left(x|m,\Omega,s\right) = \frac{2s}{\Gamma(m)}\left[\frac{m}{\Omega}\right]^m x^{(2ms-1)} e^{-\frac{m}{\Omega}x^{2s}} \qquad (3)$$

The shape adjustment parameter s controls the heaviness of the distribution tail. For $s < 1$ there are heavy tails, which vanish for $s > 1$ to a tight density function. For $m = s = 1$ the GND becomes the Rayleigh density function; for $m = 1, s \neq 0$ the function becomes the Weilbull density function; and for $m = 1$ and $s = \frac{1}{2}$ it becomes a simple exponential density function.

The estimation of the density function for the image I_2 is done for the dispersion rather than for the mean values, motivated from the view, that the Poisson particle rate follows a Gamma distribution. One can argue, that the dispersion, during the exposure for a single image pixel, increases by somewhat function with the number of arriving photons, regardless from what type of interaction they stem.

Therefore, a Gamma-like density function can be found when analyzing the SDEV of images from flat PMMA and Al phantoms. From the physical setup in Fig. 6 several panoramic phantom image scans were made with Filters 1..3. From (1), the local mean and variance of the logarithmic fraction from (2) is shown in Fig. 8, once for the unfiltered background I_1 (leftmost curve) and once for I_1, filtered by median filter (rightmost curve). Since there are no interesting details in the background, a kernel size of 9x9 was found to be appropriate to suppress the background noise.

Then a rescaled GND (3) function was fitted to the SDEV in Fig. 8. The parameters for the fit of the density function are obtained by maximum likelihood estimation (MLE). Thus, a modified *glmfit* from MATLAB fits a generalized linear model (GLM), calculates the MLE of the mean parameters, and solves the MLE for the shape parameter, which is the reciprocal of the variance parameter.

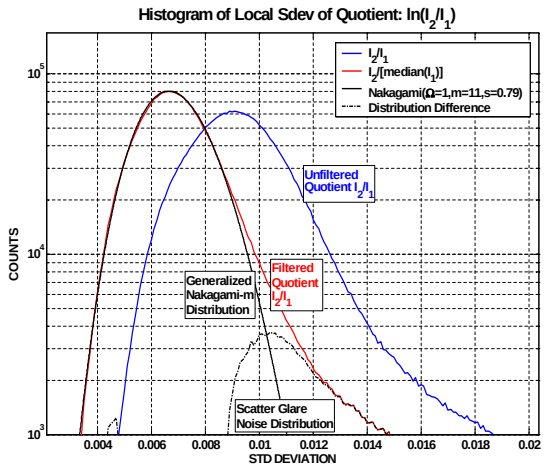

Fig. 8. Local $SDEV$ of PMMA Image. Nakagami Distribution Fitting and Scatter-Glare Error Difference.

4.2. Determining a Scatter-Glare Error Distribution

However, the GND function best fitted, does not cover the entire heavy tail of the panoramic phantom image SDEV distribution. One can argue that the difference density between the Nakagami model density function and the density function of the acquired image is probably the density of the remaining scatter-glare [7]. To verify this hypothesis, denoted H_0, the scatter-glare was directly measured by a beam stop method (see Fig. 6), such that a 3mm lead plate with holes of 3mm diameter is positioned between PMMA filter and detector. The image values located surrounding the hole areas, above the attenuation level of the lead screen are then counted accordingly to the scatter-glare distribution.

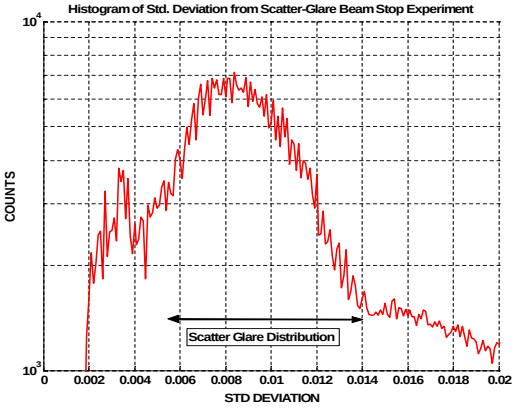

Fig. 9. $SDEV$ of Scatter-Glare: Density Error Histogram.

Fig. 9 shows a density function from the scatter-glare experiments, the hypothesis seems to be well confirmed. This leads to the support for building a spatial estimate of the diagnostic noise contribution by using the difference density from the SDEV found and the fitted GND. Therefore, the spatial noise map of scaled Gaussian random variables is formed as a GSM, by factors ξ_{xy}, and we get finally:

$$I_2 = I + \underbrace{N(0,\sigma_B)}_{Gaussian\ Bias} + \underbrace{\sum \xi_{xy}\, N(0,1)}_{Scatter-Glare\ GSM} \qquad (4)$$

Where I is the noise free image, $N(0,\sigma_B)$ is the Gaussian bias noise out of Fig.7; $\sum(..)$ represents the scatter-glare GSM; xy are pixel coordinates. Another approach [6] tries to inverse (4) to get image I noise free (see Fig. 10b).

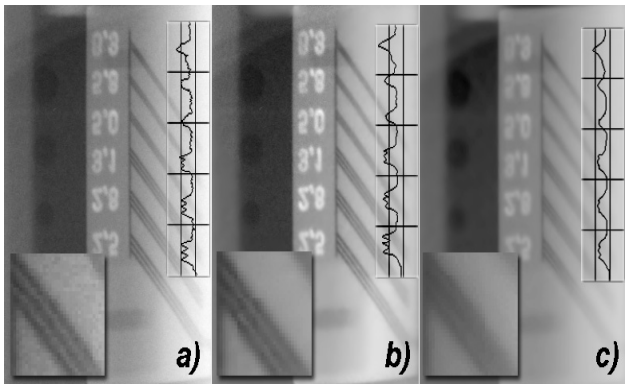

Fig. 10. A comparison of: a) source; b) proposed denoising method; c) usual denoising threshold method.

Three image slices from a MTF phantom are shown in Fig. 10: a) image is unprocessed; b) application of the proposed method and c) the threshold method. At every slide's right hand side, a vertical profiling of the sine grating patterns for MTF calculation is inserted, and at the bottom a zoomed view of the sine gratings at $2.5\ \frac{lines}{mm}$ is shown. In fact - a) is noisy, but has sharp contrast; b) shows removed noise at very good contrast; finally c) shows removed noise, but the sine grating is heavily distorted. The calculated MTF's at $2.5\ \frac{lines}{mm}$ compares with 53%, 44% and 21% for a), b), c) respectively, thus the proposed method b) preserves detail much better than the classical method c).

5. CONCLUSIONS

This paper presents a procedure for estimation of the noise in panoramic X-ray images, where the local statistics are calculated from a database of 50 images. A noise model is created, with the main purpose to achieve optimal image quality after denoising. The noise model supports the separation of the information of interest by ideas stem from Blind Source Separation. It is shown that the local standard deviation of a PMMA phantom image can be fitted well by a Generalized Nakagami Distribution (GND), where the heavily tail can be counted for the scatter-glare density. A beam-stop measurement experiment confirms that this is quantifiable.The application of the model forms a Gaussian scale mixture (GSM) and provides good results when applied for denoising (see also [6]).

6. REFERENCES

[1] Aird EGA. Basic Physics for Medical Imaging. *Heinemann, Oxford, 1988*

[2] M. Analoui. Radiographic Image Enhancement. Part II: Transform Domain Techniques. *Dentomaxillofacial Radiology, Vol 30, Issue 2 65-77, British Institute of Radiology, 2001*

[3] J. M. Boone and J. A. Seibert. An accurate method for computer generating tungsten anode x-ray spectra from 30 to 140 kV. *Medical Physics 24(11) pp.1661-1670, November 1997.*

[4] D. L. Donoho. Denoising by Soft-thresholding. *IEEE Trans. on Information Theory, Vol.41, pp.613-627, 1995*

[5] P. M. Goebel, A. N. Belbachir. An application analysis approach for noise estimation in panoramic X-ray images. *Proc. HACIPPR 2005, Veszprém, H, May, 2005:in ISBN 3-85403-192-0 Oesterreichische Computer Gesellschaft, OCG, A.*

[6] P. M. Goebel, A. N. Belbachir. Background Removal in Dental Panoramic X-ray Images by the A-Trous Multiresolution Transform. *to appear at ECCTD 2005, Cork, Ireland, 2005.*

[7] H. Holm, M. Alouini. Sum and Difference of Two Squared Correlated Nakagami Variates in Connection with the McKay Distribution. *IEEE Trans. on Comm., vol.52, No.8, Aug. 2004.*

[8] J. H. Hubbell, S. M. Seltzer Tables of X-Ray Mass Attenu. Coeff. and Mass Energy-Absorpt. Coeff. (version 1.4). *NISTIR 5632, NIST, Gaithersburg, MD, 1995.*

[9] P. Meer, J. M. Jolion, A. Rosenfeld. A Fast Parallel Algorithm for Blind Estimation of Noise Variance. *IEEE Trans. on Patt. Anal. and Machine Intel., Vol. 12, No. 2, Feb. 1990.*

[10] S. I. Olsen. Noise Variance Estimation in Images. *In 8 th Scandinavian Conf. on Image Analysis, Norway, 1993.*

[11] A. Papoulis, U. Pillai Probability, Random Variables, and Stochastic Processes. *4th ed. N. Y. McGraw-Hill, 2002..*

[12] P. M. Shankar. Ultrasonic Tissue Characterisation Using a Generalized Nakagami Model. *IEEE Trans. on Ultrasonics, Ferroel., and Frequ. Control, Vol. 48, No. 6, Nov. 2001.*

[13] E. P. Simoncelli. Statistical Models for Images: Compression, Restoration and Synthesis. *Asilomar Conf. on Signals Systems, and Computers, Pacific Grove, CA, Nov. 2-5, 1997.*

[14] J. Portilla, Eero P. Simoncelli. Image Restoration using Gaussian Scale Mixtures in the Wavelet Domain. *9th IEEE Conf on Image Proc. vol. II, Barcelona, Spain. Sep. 2003.*

[15] J. L. Starck, F. Murtagh and A. Bijaoui. Image Processing and Data Analysis: the Multiscale Approach. *Cambridge Univ. Press, 1998.*

[16] J. L. Starck, F. Murtagh Automatic noise estimation from the multiresolution support. *Publ. Astronomic Soc. of the Pacific, 110(744):193-199, 1998.*

[17] J. M. Unser, A. Aldroubi and A. Laine. Guest Editorial: Wavelets in Medical Imaging. *IEEE Transactions on Medical Imaging, vol. 22, no. 3, pp. 285-288, March 2003.*